

See discussions, stats, and author profiles for this publication at: <https://www.researchgate.net/publication/267728442>

# Theoretical Study of Electronic Properties of X-Doped (X = F, Cl, Br, I) VO<sub>2</sub> Nanoparticles for Thermochromic Energy-Saving Foils

ARTICLE in THE JOURNAL OF PHYSICAL CHEMISTRY A · OCTOBER 2014

Impact Factor: 2.69 · DOI: 10.1021/jp5092448 · Source: PubMed

---

CITATION

1

READS

43

---

## 3 AUTHORS, INCLUDING:



Qinghua Ren

Shanghai University

29 PUBLICATIONS 222 CITATIONS

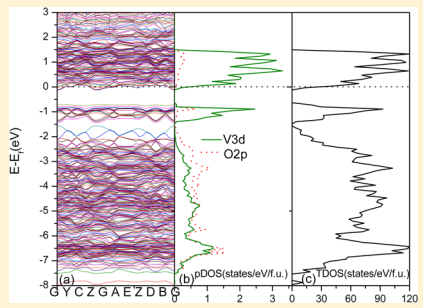
SEE PROFILE

# Theoretical Study of Electronic Properties of X-Doped (X = F, Cl, Br, I) VO<sub>2</sub> Nanoparticles for Thermochromic Energy-Saving Foils

Qinghua Ren,\*† Jinyu Wan,† and Yanfeng Gao‡

†Department of Chemistry, College of Sciences, and ‡School of Materials Science and Engineering, Shanghai University, 99 Shangda Road, Shanghai 200444, China

**ABSTRACT:** First-principles density functional theory (DFT) electronic structure calculations were carried out for the model halogen-doped VO<sub>2</sub> (M1 phase) to evaluate the effect of halogen (X = F, Cl, Br, I) doping on the band edges. The model structures of X-doped VO<sub>2</sub> with X at V site or O site were constructed on the basis of 96-atom 2 × 2 × 2 supercell of monoclinic M1 phase of VO<sub>2</sub>. Our results showed that the band gap  $E_{g2}$  for Cl-doped VO<sub>2</sub> at O1 site (0.51 eV) is smaller than that of F-doped VO<sub>2</sub> at O1 site (0.61 eV) and that of pure VO<sub>2</sub> (0.78 eV). We also investigated the substitution of chlorine, bromine, and iodine for vanadium in VO<sub>2</sub>, where the band gaps  $E_{g2}$  are 0.40, 0.45, and 0.37 eV for Cl-, Br-, and I-doped VO<sub>2</sub> at V site, respectively. The Cl-doped VO<sub>2</sub> at V site is the best one for achieving good VO<sub>2</sub> thermochromic energy-saving foils.



## 1. INTRODUCTION

It is well-known that vanadium dioxide (VO<sub>2</sub>) is one of the most explored transition metal oxides as a thermally induced phase transition material.<sup>1,2</sup> When the temperature decreases, VO<sub>2</sub> phase undergoes a phase transition from the metal to insulator phase (MIT) at 340 K. Accompanying the MIT, VO<sub>2</sub> crystal structure transforms from the rutile structure (R phase, space group P4<sub>2</sub>/mm) to the monoclinic structure (M1 phase, space group P2<sub>1</sub>/c), while its optical properties are also changed. Therefore, VO<sub>2</sub> can be used for optoelectronic devices,<sup>3</sup> solar energy transmittance modulation,<sup>4</sup> and smart windows,<sup>5,6</sup> etc.

The  $T_{\text{MIT}}$  is approximately 340 K for the pure VO<sub>2</sub>, and it should be lowered to approach the room temperature (298 K) in order to meet the requirement of the applications of VO<sub>2</sub>. There are a lot of methods to lower the transformation temperature to improve the optical transmittance and to increase the temperature coefficient of resistance characteristics, including the elemental doping,<sup>7,8</sup> stressing,<sup>9,10</sup> nonstoichiometry,<sup>11</sup> graining,<sup>12,13</sup> or a combination of these factors. The previous works demonstrated that the phase transition temperature can be reduced by doping the high valence cation (Nb<sup>5+</sup>, Mo<sup>6+</sup>, W<sup>6+</sup>, Ta<sup>5+</sup>), or increased through the low valence cation doped species (Al<sup>3+</sup>, Ti<sup>2+</sup>, Ga<sup>3+</sup>, Cr<sup>3+</sup>).<sup>6,14–17</sup> The reduced phase transition temperature keeps a high linear relationship with the concentration of the cation-doped performance. For example, tungsten is proven to be one of the most effective dopants where the transition temperature is reduced by about 28 K with increase of every 1 at. % of tungsten.<sup>18,19</sup>

In the past few years, halogen-doped TiO<sub>2</sub> species were investigated extensively, such as F-doped TiO<sub>2</sub> nanostructures exhibiting a high photocatalytic activity.<sup>20,21</sup> Yang has recently reported the model halogen-doped anatase TiO<sub>2</sub> structures in order to evaluate the effect of halogen doping on the band

edges and the photocatalytic activity of TiO<sub>2</sub> using density functional theory (DFT) calculations.<sup>22</sup> The results showed that it is energetically more favored to substitute Br or I for a Ti site than for an O site under O-rich growth conditions, but it is energetically more favorable to substitute F or Cl for an O site than for a Ti site.<sup>22</sup>

However, the halogen-doped VO<sub>2</sub> is comparatively less investigated.<sup>15</sup> Recently, Gao's group prepared F-doped VO<sub>2</sub> (M1) nanoparticles via one-pot hydrothermal synthesis and found the F-doping can decrease the phase transition temperature to 308 K at 2.93% F in VO<sub>2</sub>.<sup>23</sup> The F-doped VO<sub>2</sub> smart glass foils exhibit an increased solar-heat shielding ability and a modified comfortable color (yellow/brown) while keeping excellent solar modulation abilities and an appropriate visible transmittance. On the basis of this experimental work, we hope to theoretically explore which halogen atom doped VO<sub>2</sub> is better for thermochromic energy-saving foils and to evaluate the effect of halogen doping on the band edges. In this paper, we thoroughly investigated various halogen-doped (F, Cl, Br, I) monoclinic M1 phases of VO<sub>2</sub> using the first-principles density functional theory electronic structure calculations.

## 2. COMPUTATIONAL DETAILS

The electronic structure properties of the halogen-doped monoclinic M1 phase of VO<sub>2</sub> were studied using the periodic DFT calculations implemented in the VASP code,<sup>24,25</sup> using the local density approximation (LDA)<sup>26</sup> in the form of the Perdew–Burke–Ernzerhof (PBE) exchange-correlation functional.<sup>27</sup> Core electrons were treated with the projected

Received: September 12, 2014

Revised: October 27, 2014

Published: October 29, 2014



augmented wave (PAW) method.<sup>28</sup> The experimental structures were used for all calculations.<sup>29,30</sup> There are four V and eight O atoms in the crystallographic unit cell for the M1 phase, which were used in the calculations of pure VO<sub>2</sub>. The bulk unit calculations contained  $2 \times 2 \times 2$  super cell with 96 atoms including 32 V, 63 O, and 1 halogen or 31 V, 64 O, and 1 halogen.

Doping is widely applied to regulate the band gap. Considering that the electronegativity value of the fluorine atom is higher than that of the oxygen atom, we used fluorine substituted oxygen in VO<sub>2</sub> at the O1 site because it was energetically favored over the O2 site for the F substitution.<sup>23</sup> Gao's work showed that the F-doped VO<sub>2</sub> at the O1 site decreased the energy of the O<sub>2p</sub> states, which aided in widening the band gap between the V<sub>3d</sub> and O<sub>2p</sub>,<sup>23</sup> so we studied whether the chlorine substituted oxygen in VO<sub>2</sub> at the O1 site can give the same result. We also investigated the possibilities of substituting chlorine, bromine, or iodine for vanadium in VO<sub>2</sub> to provide an effective strategy to achieve good VO<sub>2</sub> thermochromic energy-saving foils. We compared which one is appropriate when using chlorine to substitute the oxygen atom or the vanadium site in VO<sub>2</sub>.

We used a simplified version of the rotationally invariant LDA+U method<sup>31</sup> where the adopted values of U in the LDA+U were set as 3.5 eV for the vanadium d electrons. We performed nonmagnetic calculations. The energy cutoff was put at 600 eV, and a  $4 \times 4 \times 4$  uniform Monkhorst-Pack *k* grid was used for M1 phase. The Gaussian broadening width for electronic smearing was 0.1 eV. The convergent criterion for geometrical optimization was set as  $<0.01$  eV/Å to ensure that the total energies were calculated to a convergence threshold of  $10^{-5}$  eV per cell for both functionals.

### 3. RESULTS AND DISCUSSION

We know the pure VO<sub>2</sub> (M1) phase (space group: P2<sub>1</sub>/c, *a* = 5.743 Å, *b* = 4.517 Å, *c* = 5.375 Å, and  $\beta$  = 122.61°, JCPDS No. 72-1014).<sup>29</sup> The two band gaps are illustrated in Figure 1,

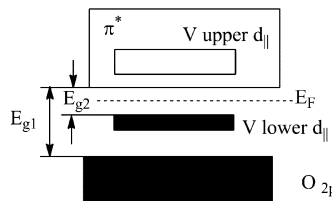


Figure 1. Outline of the two band gaps of VO<sub>2</sub> (M1 phase).

which are taken from the Goodenough's work about the electronic structure of VO<sub>2</sub>.<sup>32</sup> The lower d<sub>||</sub> band is completely

filled, and the  $\pi^*$  band is empty. E<sub>g1</sub> and E<sub>g2</sub> are associated with the band gaps between O<sub>2p</sub> and  $\pi^*$  or the lower d<sub>||</sub> and  $\pi^*$ , respectively.

The geometrical optimizations were carried out on the basis of the LDA+U method<sup>31</sup> where the optimized results are shown in Table 1 and the calculated models were illustrated in Figures 2–5. From Table 1, it can be seen that the pure VO<sub>2</sub> (eight primitive) volume was approximately 2.5% larger than that of the experimental value.<sup>29,30</sup> Compared to the optimized lattice parameters and the experimental values,<sup>30</sup> the calculated *a* value was approximately 2.2% smaller than the experimental value, while the *b* was 2.4% larger, and the *c* was 1.3% larger than the experimental values. The optimized angle  $\alpha$  and  $\gamma$  were about 90°, while  $\beta$  was 121.70° which had little difference from the experimental value of 122.6°. From these results, it can be concluded that the LDA+U method<sup>31</sup> is feasible for our model calculations.

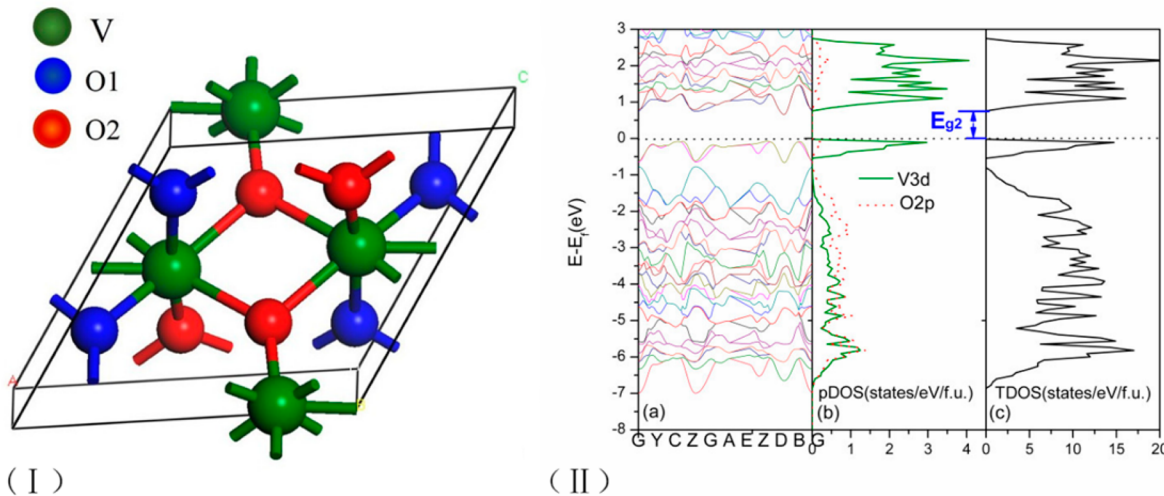
For the 2.93% X-doped VO<sub>2</sub>, when X = F and one O atom substituted at O1 site, the cell volume increased from 968.00 to 969.41 Å<sup>3</sup>, which was an approximately 0.1% increase in volume. The optimized lattice parameters *a*, *b*, and *c* varied little from 11.246, 9.277, and 10.906 Å to 11.249, 9.285, and 10.905 Å for F-doping to the substitute O atom, respectively. However, if X is Cl to substitute one O atom at O1 site, the cell volume increased from 968.00 to 979.14 Å<sup>3</sup>, which increased more in volume about 1.2%. The optimized lattice parameters *a*, *b*, and *c* were also increased more. When X is Cl, Br, I to substitute one V atom, the cell volumes increased from 968.00 to 979.89, 980.29, and 980.62 Å<sup>3</sup> for Cl-, Br-, I-doping, respectively, which are closer to the volume when Cl-doped VO<sub>2</sub> for O1 site. The optimized lattice parameters for three of them to substitute one V atom are closer, but are little different from that of Cl-doped VO<sub>2</sub> for O1 site.

The calculated unit cell structure of the monoclinic pure VO<sub>2</sub> is shown in Figure 2I. The band structure, total density of states (TDOS), and partial density of states (pDOS) for V(3d) and O(2p) of the unit cell of the M1 VO<sub>2</sub> were illustrated in Figure 2II. The band gap E<sub>g2</sub> between the occupied states below the Fermi level and the unoccupied states above the Fermi level is 0.78 eV for the monoclinic pure VO<sub>2</sub>, which describes the insulating properties of the monoclinic structure of vanadium dioxide. This is consistent with the experimental results and other calculated results.<sup>33,34,31</sup>

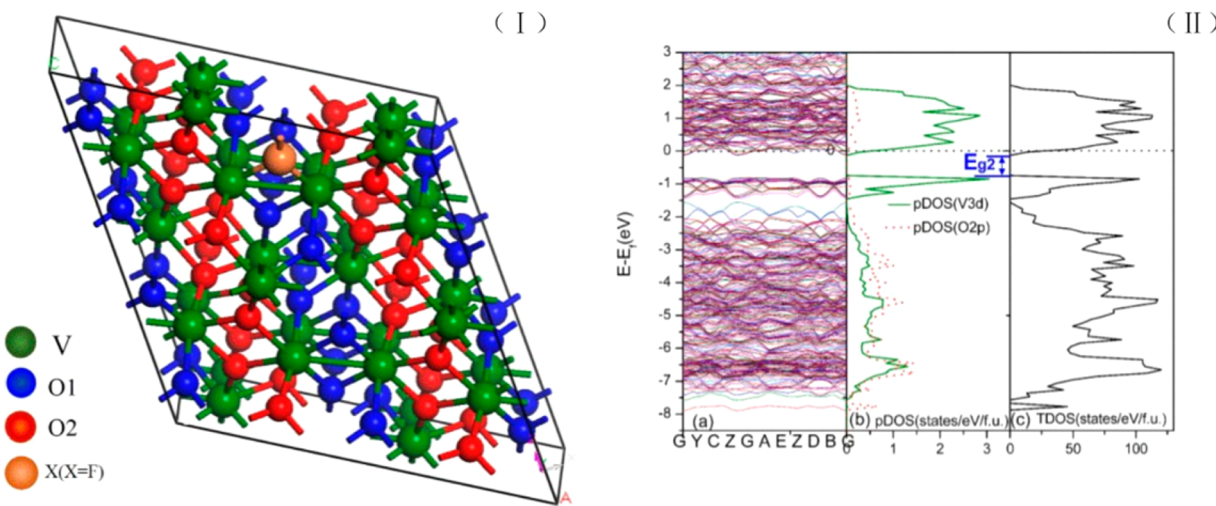
From Figure 2II, the V(3d) states and O(2p) states are the principal components of the TDOS. The data of Figure 2IIa,b demonstrate that the first valence band is from the Fermi level (0.eV) to -0.54 eV and the second valence band is from -0.80 to -6.86 eV, so the calculated band gap between the first and second valence bands was 0.26 eV.

Table 1. Optimized Geometries of Pure and X-Doped (F, Cl, Br, I) VO<sub>2</sub> Compared to the Experimental Values

	<i>a</i> /Å	<i>b</i> /Å	<i>c</i> /Å	$\alpha$ /deg	$\beta$ /deg	$\gamma$ /deg	<i>V</i> /Å <sup>3</sup>	
<b>M1-Phase</b>								
V <sub>32</sub> O <sub>64</sub>	11.486	9.034	10.750	90	122.60	90	939.728	expt <sup>29</sup>
V <sub>32</sub> O <sub>64</sub>	11.506	9.052	10.766	90	122.60	90	944.56	expt <sup>30</sup>
V <sub>32</sub> O <sub>64</sub>	11.246	9.277	10.906	90.0	121.70	90.0	968.00	this calc
V <sub>32</sub> O <sub>63</sub> F	11.249	9.285	10.905	89.82	121.67	89.97	969.41	this calc
V <sub>32</sub> O <sub>63</sub> Cl	11.276	9.314	10.958	90.68	121.70	89.94	979.14	this calc
V <sub>31</sub> ClO <sub>64</sub>	11.365	9.280	10.992	90.42	122.30	89.62	979.89	this calc
V <sub>31</sub> BrO <sub>64</sub>	11.383	9.274	10.983	90.36	122.28	89.56	980.29	this calc
V <sub>31</sub> IO <sub>64</sub>	11.340	9.301	10.943	89.97	121.85	90.02	980.62	this calc



**Figure 2.** (I) Calculated unit cell structure of pure  $\text{VO}_2$ . (II) The band structure, total density of states (TDOS), and partial density of states (pDOS) for V(3d) and O(2p).



**Figure 3.** (I) Calculated  $2 \times 2 \times 2$  supercell structure for F-doped  $\text{VO}_2$  at O1 site. (II) The band structure, total density of states (TDOS), and partial density of states (pDOS) for V(3d) and O(2p).

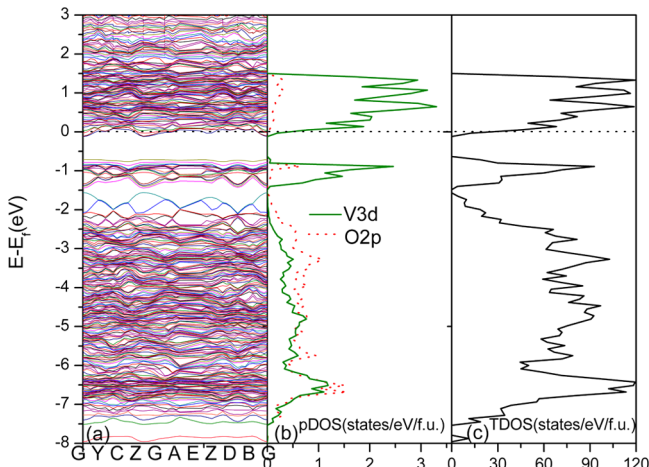


**Figure 4.** Band structure, total density of states (TDOS), and partial density of states (pDOS) for Cl-doped  $\text{VO}_2$  at O1 site.

The optimized structures of X-doped  $\text{VO}_2$  with X at O site were constructed on the basis of 96-atoms  $2 \times 2 \times 2$  supercell, including 32 V, 63O, and 1X atom.  $\text{VO}_2$  (M1) has two different O sites labeled as O1 (blue) and O2 (red), which can be seen clearly in Figure 2I. As far as we know, the O1 site was energetically favored over the O2 site for F substitution.<sup>23</sup> So, we only considered the halogen atom to substitute O atom at O1 site. Figure 3I showed that the calculated structure of F-doped  $\text{VO}_2$  at O1 site and Figure 3II illustrated the band structure, total density of states (TDOS), and partial density of states (pDOS) for V(3d) and O(2p). From Figure 3II, the Fermi level for the F-doped  $\text{VO}_2$  is moved into the conduction band. Compared to the Fermi level for the pure  $\text{VO}_2$  shown in Figure 2II, it means that the F-doped  $\text{VO}_2$  should have a stronger metallicity than the pure  $\text{VO}_2$  (M1). The band gap of  $E_{g2}$  between the occupied states and the unoccupied states shown in Figure 3II is 0.61 eV, which is smaller than that of pure  $\text{VO}_2$ . Hu<sup>35</sup> has studied the electronic properties of Mg-doped  $\text{VO}_2$  using DFT calculations with HSE hybrid functional and reported that the values of  $E_{g2}$  are 0.72 and 1.01 eV for the  $\text{Mg}/(\text{V}+\text{Mg}) = 0.125$  and 0.25, respectively. Li's work<sup>36</sup> also

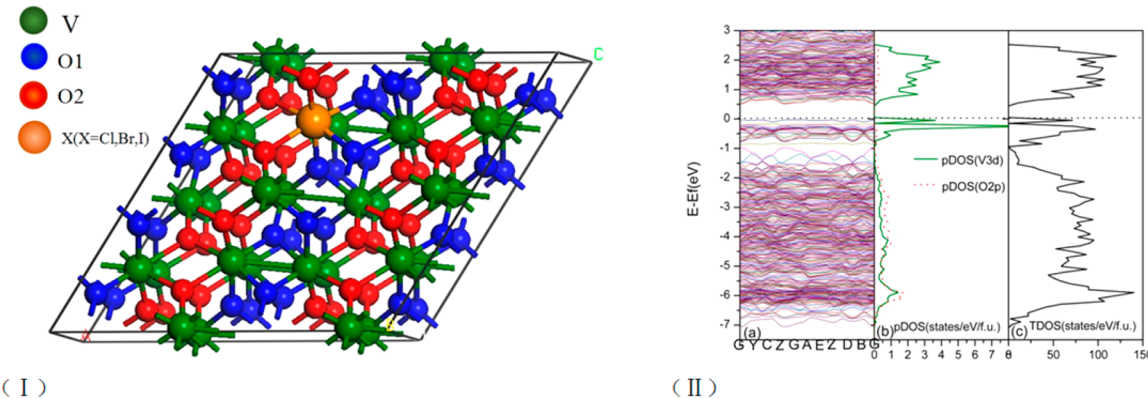


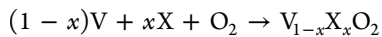
**Figure 5.** (I) Calculated  $2 \times 2 \times 2$  supercell structure for X-doped  $\text{VO}_2$  at V site. (II) The band structure, total density of states (TDOS), and partial density of states (pDOS) for V(3d) and O(2p).

proved that Mg-doped thermochromic  $\text{VO}_2$  thin films display strong band gap widening proportionately to the Mg content. It can be seen that the Mg-doped  $\text{VO}_2$  increased the band gap of  $E_{g2}$ , but the F-doped  $\text{VO}_2$  for our case decreased the band gap of  $E_{g2}$ .

Similarly, the Cl-doped  $\text{VO}_2$  with the Cl atom to substitute O atom at O1 site was calculated. Figure 4 showed that the band structure, total density of states (TDOS), and partial density of states (pDOS) for V(3d) and O(2p) for Cl-doped  $\text{VO}_2$  at O1 site. From Figure 4, the Fermi level for the Cl-doped  $\text{VO}_2$  is also moved into the conduction band, which means the Cl-doped  $\text{VO}_2$  also shows a higher metallicity. The band gap of  $E_{g2}$  (not shown in Figure 4, the same place as that in Figure 3) is 0.51 eV, which is smaller than that of F-doped  $\text{VO}_2$  at O1 site (0.61 eV) and that of pure  $\text{VO}_2$  (0.78 eV). The change of the transition energies from the insulator phase to the metal phase is directly related to the variation of band gap.<sup>37,38</sup> In the high-temperature metal phase, the band gap of  $E_{g2}$  is reduced to zero. The decrease of band gap will result in the decrement of transition energies.<sup>37</sup> It means the Cl-doped  $\text{VO}_2$  at O1 site is better than the F-doped  $\text{VO}_2$  at O1 site for the decrease of the phase transition temperature. Gao's work also proved that the band gap for F-doped  $\text{VO}_2$  becomes smaller and results in the lower phase transition temperature as compared to the pure  $\text{VO}_2$ .<sup>23</sup>

The optimized structures of X-doped  $\text{VO}_2$  with X = Cl, Br, I at V site (96-atoms  $2 \times 2 \times 2$  supercell including 31 V, 64 O and 1 halogen) were illustrated in Figure S1. The band structure, total density of states (TDOS), and partial density of states (pDOS) for V(3d) and O(2p) for X-doped  $\text{VO}_2$  at V site are shown in Figure SII. The band gaps of  $E_{g2}$  are 0.40, 0.45, and 0.37 eV for Cl-, Br-, I-doped  $\text{VO}_2$  at V site, respectively.

In order to evaluate the formation Helmholtz free energy of  $\text{V}_{1-x}\text{X}_x\text{O}_2$  (here, X-doped  $\text{VO}_2$  with X at V site), the following equation was used:



For the 96-atom  $2 \times 2 \times 2$  supercell, the formation Helmholtz free energy of  $\text{V}_{31}\text{XO}_{64}$  at 0 K was evaluated as

$$\Delta_f U[\text{V}_{31}\text{XO}_{64}] = U[\text{V}_{31}\text{XO}_{64}] - 31U[\text{V}] - U[\text{X}] - 32U[\text{O}_2]$$

where the  $U$ 's in right side are free energies evaluated from DFT calculations of the corresponding components. The calculated results are  $-163.115$  eV for  $\text{V}_{31}\text{ClO}_{64}$ ,  $-162.975$  eV

for  $\text{V}_{31}\text{BrO}_{64}$ , and  $-164.051$  eV for  $\text{V}_{31}\text{IO}_{64}$ . It can be seen that the formation Helmholtz free energies of  $\text{V}_{31}\text{XO}_{64}$  with Cl-, Br-, I-doped  $\text{VO}_2$  with X at V site are Br ( $-162.975$  eV) > Cl ( $-163.115$  eV) > I ( $-164.051$  eV). It stays in line with the results of band gaps of  $E_{g2}$ , Br (0.45 eV) > Cl (0.40 eV) > I (0.37 eV), which means the doping becomes less difficult in the order Br < Cl < I for X-doped  $\text{VO}_2$  at V site. The results are different from the results of Yang about the halogen-doped anatase  $\text{TiO}_2$  structures.<sup>22</sup> It showed that the doping becomes less difficult in the order F < Cl < Br < I for X-doped  $\text{TiO}_2$  at Ti site and becomes more difficult in the order F < Cl < Br < I for X-doped  $\text{TiO}_2$  at O site.

Considering that the iodine atom has a color and it is not a good choice to be used as the doping atom for the "smart glass" films, the Cl is the best doping atom for  $\text{VO}_2$  at V site. Furthermore, the band gap of  $E_{g2}$  for Cl-doped  $\text{VO}_2$  at V site (0.40 eV) is also smaller than that of Cl-doped  $\text{VO}_2$  at O1 site (0.51 eV), so the Cl-doped  $\text{VO}_2$  at V site is the best one for achieving good  $\text{VO}_2$  thermochromic energy-saving foils. All X-doped (F, Cl, Br, I)  $\text{VO}_2$  decreased the band gap, which was different from the Mg-doped thermochromic  $\text{VO}_2$  widening the band gap.<sup>35,36</sup>

## 4. CONCLUSION

The present paper thoroughly investigated various halogen-doped (F, Cl, Br, I) monoclinic M1 phases of  $\text{VO}_2$  using the first-principles density functional theory electronic structure calculations. We studied the fluorine and chlorine substituted oxygen in  $\text{VO}_2$  at the O1 site. The band gap of  $E_{g2}$  for Cl-doped  $\text{VO}_2$  at O1 site (0.51 eV) is smaller than that of F-doped  $\text{VO}_2$  at O1 site (0.61 eV) and that of pure  $\text{VO}_2$  (0.78 eV). We also investigated the substituting of chlorine, bromine, and iodine for vanadium in  $\text{VO}_2$ , where the band gaps of  $E_{g2}$  are 0.40, 0.45, and 0.37 eV for Cl-, Br-, I-doped  $\text{VO}_2$  at V site, respectively. It can be concluded that the Cl-doped  $\text{VO}_2$  at V site is the best one for achieving good  $\text{VO}_2$  thermochromic energy-saving foils.

## ■ AUTHOR INFORMATION

### Corresponding Author

\*E-mail: qinghua.ren@shu.edu.cn. Phone: +86-21-66132404. Fax: +86-21-66134594.

### Notes

The authors declare no competing financial interest.

## ACKNOWLEDGMENTS

This work is supported by Shanghai Higher Education Connotation Construction “085” Project “Materials Genome Engineering” Funding (B.58-B111-12-101, B.58-B111-12-103) and State Outstanding Young Scholars (NSFC, 51325203) and the high performance computing platform of Shanghai University.

## REFERENCES

- (1) Morin, F. J. Oxides Which Show a Metal-to-Insulator Transition at the Neel Temperature. *Phys. Rev. Lett.* **1959**, *3*, 34–36.
- (2) Park, J. H.; Coy, J. M.; Kasirga, T. S.; Huang, C.; Fei, Z.; Hunter, S.; Cobden, D. H. Measurement of a Solid-State Triple Point at the Metal-Insulator Transition in  $\text{VO}_2$ . *Nature* **2013**, *500*, 431–434.
- (3) Kasirga, T. S.; Sun, D.; Park, J. H.; Coy, J. M.; Fei, Z. Y.; Xu, X. D.; Cobden, D. H. Photoresponse of a Strongly Correlated Material Determined by Scanning Photocurrent Microscopy. *Nat. Nanotechnol.* **2012**, *7*, 723–727.
- (4) Chang, S. J.; Hong, W. K.; Kim, H. J.; Lee, J. B.; Yoon, J.; Ko, H. C.; Huh, Y. S. Probing the Photothermally Induced Phase Transitions in Single-Crystalline Vanadium Dioxide Nanobeams. *Nanotechnology* **2013**, *24*, 345701/1–345701/7.
- (5) Granqvist, C. G. Spectrally Selective Coatings for Energy Efficiency and Solar Applications. *Phys. Scr.* **1985**, *32*, 401–407.
- (6) Li, S. Y.; Niklasson, G. A.; Granqvist, C. G. Thermochromic Fenestration with  $\text{VO}_2$ -Based Materials: Three Challenges and How They Can Be Met. *Thin Solid Films* **2012**, *520*, 3823–3828.
- (7) Burkhardt, W.; Christmann, T.; Franke, S.; Kriegseis, W.; Meister, D.; Meyer, B. K.; Niessner, W.; Schalch, D.; Scharmann, A. Tungsten and Fluorine Co-doping of  $\text{VO}_2$  Films. *Thin Solid Films* **2002**, *402*, 226–231.
- (8) Mai, L. Q.; Hu, B.; Hu, T.; Chen, W.; Gu, E. D. Electrical Property of Mo-Doped  $\text{VO}_2$  Nanowire Array Film by Melting-Quenching Sol-Gel Method. *J. Phys. Chem. B* **2006**, *110*, 19083–19086.
- (9) Muraoka, Y.; Hiroi, Z. Metal–Insulator Transition of  $\text{VO}_2$  Thin Films Grown on  $\text{TiO}_2$  (001) and (110) Substrates. *Appl. Phys. Lett.* **2002**, *80*, 583–585.
- (10) Tsai, K. Y.; Chin, T. S.; Shieh, H. P. D.; Ma, C. H. Effect of As-Deposited Residual Stress on Transition Temperatures of  $\text{VO}_2$  Thin Films. *J. Mater. Res.* **2004**, *19*, 2306–2314.
- (11) Griffith, G. H.; Eastwood, H. K. Influence of Stoichiometry on the Metal-Semiconductor Transition in Vanadium Dioxide. *J. Appl. Phys.* **1974**, *45*, 2201–2206.
- (12) Chen, S.; Ma, H.; Dai, J.; Yi, X. Nanostructured Vanadium Dioxide Thin Films with Low Phase Transition Temperature. *Appl. Phys. Lett.* **2007**, *90*, 101117/1–101117/3.
- (13) Whittaker, L.; Jaye, C.; Fu, Z.; Fischer, D. A.; Banerjee, S. Depressed Phase Transition in Solution-Grown  $\text{VO}_2$  Nanostructures. *J. Am. Chem. Soc.* **2009**, *131*, 8884–8894.
- (14) Lu, S.; Hou, L.; Gan, F. Surface Analysis and Phase Transition of Gel-Derived  $\text{VO}_2$  Thin Films. *Thin Solid Films* **1999**, *353*, 40–44.
- (15) Burkhardt, W.; Christmann, T.; Meyer, B. K.; Niessner, W.; Schalch, D.; Scharmann, A. W.- and F-Doped  $\text{VO}_2$  Films Studied by Photoelectron Spectrometry. *Thin Solid Films* **1999**, *345*, 229–235.
- (16) Ghedira, M.; Vincent, H.; Marezio, M.; Launay, J. C. Structural Aspects of the Metal-Insulator Transitions in  $\text{V}_{0.985}\text{Al}_{0.015}\text{O}_2$ . *J. Solid State Chem.* **1977**, *22*, 423–438.
- (17) Villeneuve, G.; Bordet, A.; Casalot, A.; Hagenmuller, P. Propriétés Physiques et Structurales de la Phase  $\text{Cr}_x\text{V}_{1-x}\text{O}_2$ . *Mater. Res. Bull.* **1971**, *6*, 119–130.
- (18) Shibuya, K.; Kawasaki, M.; Tokura, Y. Metal-Insulator Transition in Epitaxial  $\text{V}_{1-x}\text{W}_x\text{O}_2$  ( $0 \leq x \leq 0.33$ ) Thin Films. *Appl. Phys. Lett.* **2010**, *96*, 022102/1–022102/3.
- (19) Mao, M.; Huang, W.; Zhang, Y.; Yan, J.; Luo, Y.; Shi, Q.; Cai, J. Study on Phase Transition Property of Tungsten-doped Vanadium Dioxide Thin Film at Terahertz Range. *Wuji Cailiao Xuebao* **2012**, *27*, 891–896.
- (20) Yu, J. C.; Yu, J.; Ho, W.; Jiang, Z.; Zhang, L. Effects of  $\text{F}^-$  Doping on the Photocatalytic Activity and Microstructures of Nanocrystalline  $\text{TiO}_2$  Powders. *Chem. Mater.* **2002**, *14*, 3808–3816.
- (21) Wu, G.; Wang, J.; Thomas, D. F.; Chen, A. Synthesis of F-Doped Flower-Like  $\text{TiO}_2$  Nanostructures with High Photoelectrochemical Activity. *Langmuir* **2008**, *24*, 3503–3509.
- (22) Yang, K.; Dai, Y.; Huang, B.; Whangbo, M. H. Density Functional Characterization of the Band Edges, the Band Gap States, and the Preferred Doping Sites of Halogen-Doped  $\text{TiO}_2$ . *Chem. Mater.* **2008**, *20*, 6528–6534.
- (23) Dai, L.; Chen, S.; Liu, J.; Gao, Y.; Zhou, J.; Chen, Z.; Cao, C.; Luo, H.; Kanahira, M. F-Doped  $\text{VO}_2$  Nanoparticles for Thermochemical Energy-Saving Foils with Modified Color and Enhanced Solar-Heat Shielding Ability. *Phys. Chem. Chem. Phys.* **2013**, *15*, 11723–11729.
- (24) Kresse, G.; Furthmüller, J. Efficient Iterative Schemes for *ab Initio* Total-Energy Calculations Using a Plane Wave Basis Set. *Phys. Rev. B* **1996**, *54*, 11169–11186.
- (25) Kresse, G.; Furthmüller, J. Efficiency of *ab-Initio* Total Energy Calculations for Metals and Semiconductors Using a Plane-Wave Basis Set. *Comput. Mater. Sci.* **1996**, *6*, 15–50.
- (26) Perdew, J. P.; Wang, Y. Accurate and Simple Analytic Representation of the Electron-gas Correlation Energy. *Phys. Rev. B* **1992**, *45*, 13244–13249.
- (27) Perdew, J. P.; Burke, K.; Ernzerhof, M. Generalized Gradient Approximation Made Simple. *Phys. Rev. Lett.* **1996**, *77*, 3865–3868 Erratum **1996**, *77*, 1396–1396.
- (28) Bloechl, P. E. Projector Augmented-Wave Method. *Phys. Rev. B* **1994**, *50*, 17953–17979.
- (29) Andersson, G. Studies on Vanadium Oxides II. The Crystal Structure of Vanadium Dioxide. *Acta Chem. Scand.* **1956**, *10*, 623–628.
- (30) Rogers, K. D. An X-ray Diffraction Study of Semiconductor and Metallic Vanadium Dioxide. *Powder Diffr.* **1993**, *8*, 240–244.
- (31) Liebsch, A.; Ishida, H.; Bihlmayer, G. Coulomb Correlations and Orbital Polarization in the Metal-Insulator Transition of  $\text{VO}_2$ . *Phys. Rev. B* **2005**, *71*, 085109/1–085109/5.
- (32) Goodenough, J. B. The Two Components of the Crystallographic Transition in  $\text{VO}_2$ . *J. Solid. State. Chem.* **1971**, *3*, 490–500.
- (33) Rana, R. S.; Nolte, D. D.; Chudnovskii, F. A. Optical Bistability from a Thermodynamic Phase Transition in Vanadium Dioxide I. *Opt. Lett.* **1992**, *17*, 1385–1387.
- (34) Gao, Y.; Wang, S.; Luo, H.; Dai, L.; Cao, C.; Liu, Y.; Chen, Z.; Kanahira, M. Enhanced Chemical Stability of  $\text{VO}_2$  Nanoparticles by the Formation of  $\text{SiO}_2/\text{VO}_2$  Core/shell Structures and the Application to Transparent and Flexible  $\text{VO}_2$ -Based Composite Foils with Excellent Thermochromic Properties for Solar Heat Control. *Energy Environ. Sci.* **2012**, *5*, 6104–6110.
- (35) Hu, S.; Li, S. Y.; Ahuja, R.; Granqvist, C. G. Optical Properties of Mg-doped  $\text{VO}_2$ : Absorption Measurements and Hydrid Functional Calculations. *Appl. Phys. Lett.* **2012**, *101*, 201902/1–201902/4.
- (36) Li, S. Y.; Mlyuka, N. R.; Primetzhofer, D.; Hallen, A.; Possnert, G.; Niklasson, G. A.; Granqvist, C. G. Bandgap Widening in Thermochromic Mg-Doped  $\text{VO}_2$  Thin Films: Quantitative Data Based on Optical Absorption. *Appl. Phys. Lett.* **2013**, *103*, 161907/1–161907/4.
- (37) Li, W. W.; Yu, Q.; Liang, J. R.; Jiang, K.; Hu, Z. G.; Liu, J.; Chen, H. D.; Chu, J. H. Intrinsic Evolutions of Optical Functions, Band Gap, and Higher-Energy Electronic Transitions in  $\text{VO}_2$  Film near the Metal-Insulator Transition Region. *Appl. Phys. Lett.* **2011**, *99*, 241903/1–241903/3.
- (38) Liu, W. T.; Cao, J.; Fan, W.; Hao, Z.; Martin, M. C.; Shen, Y. R.; Wu, J.; Wang, F. Intrinsic Optical Properties of Vanadium Dioxide near the Insulator-Metal Transition. *Nano Lett.* **2011**, *11*, 466–470.